Biological Conservation 237 (2019) 125–132

Contents lists available at ScienceDirect

Biological Conservation

journal homepage: www.elsevier.com/locate/biocon

Measuring the spectral signature of polar bears from a drone to improve their detection from space

Dominique Chabot[a,*], Seth Stapleton[b], Charles M. Francis[c]

[a] droneMetrics, 7 Tauvette Street, Ottawa, Ontario K1B 3A1, Canada
[b] Department of Fisheries, Wildlife and Conservation Biology, University of Minnesota, 2003 Buford Circle, St. Paul, MN 55108, USA
[c] Canadian Wildlife Service, Environment and Climate Change Canada, 1125 Colonel By Drive, Ottawa, Ontario K1A 0H3, Canada

ARTICLE INFO

Keywords:
Climate change
Conservation
Image analysis
Polar biology
Remote sensing
Unmanned aircraft

ABSTRACT

The increasing spatial resolution of earth observation satellites is creating new opportunities to survey wildlife. Satellites could be particularly valuable for surveying polar bears (*Ursus maritimus*) because of their remote circumpolar distribution and status of concern in the face of Arctic warming. However, the white coloration of bears does not contrast well with sea ice or snow in panchromatic imagery. We took advantage of the close-range observation capabilities of a drone to determine the spectral signature of polar bears as they would appear in multispectral satellite imagery, capturing low-altitude (≤100 m) multispectral images of bears in natural landscapes in Churchill, Manitoba, Canada. The bears' spectral curves were similar to those previously measured from pelts, with reflectance increasing with wavelength through the visible spectrum, although live bears had higher reflectance than pelts in the red-edge and near-infrared region. Bears had sufficiently consistent reflectance across the overhead surface of their body that ≥50% of pixels comprising each subject could be confidently matched to its core spectral signature, boding well for detection in coarser satellite imagery. Bears were clearly distinguishable from snow by their much lower reflectance in the blue and green region, but could potentially be confounded with large bright boulders. Currently available multispectral satellite imagery may still be too coarse (1.2 m/pixel) to reliably detect polar bears on sea ice, but resolution will likely continue to increase in future systems. Drones are a useful tool to resolve the spectral signature of wildlife species that could potentially be detected in satellite imagery.

1. Introduction

Satellite-based remote sensing technologies are rapidly advancing and increasingly being used to monitor and model the abundance and distribution of wildlife species (He et al., 2015). The tremendous value of earth observation satellites for environmental and ecological monitoring over vast swaths of the Earth's surface has long been recognized (Kerr and Ostrovsky, 2003), but only recently has satellite imagery achieved sufficiently high spatial resolutions to enable direct detection of wild animals or their signs. One of the first such studies involved detection of colonies of emperor penguins (*Aptenodytes forsteri*) (Barber-Meyer et al., 2007). Subsequently, an increasing number of papers have reported detection of a variety of wildlife species in several parts of the world using satellite imagery (LaRue et al., 2017), including other penguins species (Lynch et al., 2012), flamingos (Sasamal et al., 2008), masked boobies (*Sula dactylatra*) (Hughes et al., 2011), seals (LaRue et al., 2011; McMahon et al., 2014), large African mammals (Yang et al., 2014; Xue et al., 2017), polar bears (*Ursus maritimus*) (Stapleton et al., 2014a; LaRue et al., 2015), whales (Fretwell et al., 2014) and albatrosses (Fretwell et al., 2017).

The polar bear is a species for which satellite-based monitoring could be particularly attractive for several reasons. Polar bears occupy large geographic areas at low densities in remote locations throughout the Arctic and, as a result, can be challenging and expensive to monitor using traditional techniques such as mark-recapture methods (Lunn et al., 2016; Regehr et al., 2018) or low-level aerial surveys (Stapleton et al., 2014b). Both approaches are expensive, labour-intensive, and dangerous—several researchers have been killed or injured studying polar bears in the Arctic (Stirling, 2011). Moreover, several conservation concerns related to polar bears necessitate an increase in monitoring frequency and geographic scope. Shifts in the distribution and timing of sea ice melt affect where and when bears can hunt and may affect population health (Laidre et al., 2018). The frequency of human-bear conflicts is increasing (Schmidt and Clark, 2018), at least partly

* Corresponding author.
E-mail address: dominique.chabot@mail.mcgill.ca (D. Chabot).

https://doi.org/10.1016/j.biocon.2019.06.022
Received 14 February 2019; Received in revised form 2 May 2019; Accepted 19 June 2019
Available online 06 July 2019

related to bears spending more time on land due to changes in patterns of sea ice breakup, including near human settlements.

To date, studies on the detection of polar bears in satellite imagery have focussed on identifying bears when they are on land, such that their white color contrasts strongly with the background (Stapleton et al., 2014a; LaRue et al., 2015; LaRue and Stapleton, 2018). Even in this situation, there may be difficulty confidently identifying potential targets due to the occurrence of other white or bright objects and features of similar size to bears in the landscape, particularly those that are transient, such as patches of snow, or clumps of foam that accumulate on the edges of water. LaRue et al. (2015) found that the bears' albedo was insufficiently distinct to isolate them from confounding features in single-band panchromatic imagery. However, a multi-temporal image differencing approach proved effective in these studies for identifying polar bears based on the assumption that a bear should not be found in the same spot at two different time periods (Stapleton et al., 2014a; LaRue and Stapleton, 2018).

Despite some successes in detection of polar bears on land using satellite imagery, conducting surveys of snow- and ice-covered areas is of interest for several reasons. First, bears in most populations remain on sea ice year-round. Few populations are seasonally ice-free, and of these, polar bears concentrate on islands where they potentially could be surveyed during the ice-free period in only a few areas. LaRue and Stapleton (2018), for example, commissioned imagery for all 6700 km^2 of Wrangel Island, but only obtained cloud-free imagery for 9% of the island. At other times of the year, bears in seasonally ice-free populations are distributed at low densities across vast expanses of sea ice.

Use of multispectral imagery has the potential to expand the geographic areas in which remote sensing could be used to detect polar bears to include the sea ice where they spend much of the year. Grojean et al. (1980) and Leblanc et al. (2016) showed that the spectral reflectance curves of polar bear pelts are quite different from clean snow, with much higher absorption at short wavelengths (ultraviolet and visible) and greater reflectance at longer wavelengths approaching and into the short-wave infrared region. Although LaRue et al. (2015) found the multispectral satellite imagery they analyzed was too coarse (2.4 m/pixel) to resolve objects the size of bears, the spatial resolution of commercially available multispectral satellite imagery has since increased and will presumably continue to increase going forward, thereby expanding applications for its use.

We undertook a study to assess the feasibility of using multispectral imagery to detect and identify wild polar bears against a variety of backgrounds. Previous studies of spectral reflectance were limited to dried pelts that may differ from live animals due to aging and preservation treatments (Leblanc et al., 2016). Furthermore, these studies limited their comparisons to clean snow; information is lacking on how the reflectance of potential confounding features in a natural environment compares to that of polar bears. For this study, we took advantage of emerging drone aircraft technology—which enables unprecedented close-range observation, including from a vertical angle, of otherwise difficult-to-approach wildlife (Chabot and Bird, 2015)—to collect aerial multispectral imagery of live, wild polar bears in a natural habitat setting. Our aim was to collect and analyze imagery of multiple bears along with a variety of potential confounding features in the surrounding landscape to provide additional information that could aid in the identification of polar bears in satellite imagery.

2. Materials and methods

Data were collected from 27 to 31 October 2014 in and around the Cape Churchill Wildlife Management Area near Churchill, Manitoba, Canada. Large numbers of polar bears from the Western Hudson Bay population concentrate in this area from late summer until the bay freezes over in early winter (Regehr et al., 2007). Daytime temperatures during data collection ranged from −1 to −7 °C, wind speeds varied from ~10–40 km/h, and sky conditions were cloudy/overcast with the exception of 31 October when there was a mix of sun and cloud.

A Responder drone helicopter (ING Robotic Aviation, Ottawa, ON, Canada) was used to carry a Mini-MCA6 multispectral camera array (Tetracam, Chatsworth, CA, USA) that recorded 1280 × 1024-pixel images in six 10-nm-wide spectral bands centered at 470 nm (blue), 550 nm (green), 660 nm (red), 690 nm (red-edge), 710 nm (red-edge) and 810 nm (near-infrared). The field team travelled along the main roads or the roads in the management area during daylight hours, opportunistically searching for resting bears. Surveys were conducted from a Tundra Buggy bus or a pickup truck. When a bear was spotted, the vehicle approached along the road to a reasonable proximity, usually within 100–300 m of the bear, although one flight was initiated > 800 m away. The drone was deployed from either the road or the roof of the vehicle and flown toward the bear via manual radio-control, initially approaching at an altitude of ~100 m above ground level, with the camera continuously capturing images at 2-second intervals. A live video feed from the camera transmitted to the drone's ground control station enabled the operators to maneuver the drone into a hovering position directly above the bear. The drone was then slowly descended to capture increasingly fine-scale images, down to a minimum altitude of ~30 m, and finally flown back to the location of the field crew and landed on the road. Flights lasted 5–10 min from takeoff to landing. Prior to each flight, a white Teflon radiometric calibration tile (Tetracam) was photographed on the ground under ambient light conditions for subsequent normalization of spectral measurements made in images during each flight.

Polar bear images were captured in a total of 14 flights, generally involving a single bear, although one flight captured imagery of an adult female with two cubs. The first bear imaged on 27 October stood up and walked away from its resting spot shortly after we began collecting imagery, evidently disturbed by the drone. However, all other bears remained where they were first observed, although they occasionally shifted their posture or looked up at the drone while it hovered overhead. Collectively, the bears were imaged against a variety of landscape backgrounds (example images provided in Figs. A1–A3 in appendix), which can be broadly categorized as those containing significant amounts of rocks and gravel (27 October), those dominated by vegetation (28 October, with most vegetation dead or senescing at that time), and those dominated by snow (30 and 31 October) following a snowfall on 29 October.

Raw individual images from each of the camera's channels were spatially aligned and processed into 8-bit multiband (six bands per image) TIFF format with Tetracam PixelWrench2 v1.2.4. All subsequent image analyses were performed with ENVI v5.4.1 (Exelis/Harris Geospatial, Boulder, CO, USA) and its accompanying scripting application, IDL v8.6.1. We reviewed the images from each flight, setting aside all images containing the bear(s) (ranging from 8 to 163 images per flight) as well as an image of the calibration tile. Among the images of bears, we selected six from each flight to make spectral reflectance measurements, with the exception of one flight during which only four sufficiently clear images of the bear were captured, and another flight performed very early in the morning that produced unworkably dark imagery. Image selection was primarily constrained by sharpness, as many images were blurry due to the motion of the drone. To the extent possible, we selected images taken from varying altitudes during each flight and showing the target bear in varying postures. We also avoided images in which the bear was very close to the edge of the frame where it could be darkened by lens vignetting.

To make spectral measurements from the calibration tile and bears, we used the 'Region of Interest' tool to manually draw a polygon delineating the inner boundary of the subject. Because of subtle spatial misalignment among the camera's channels, a separate polygon was drawn in each spectral band for each image. We then computed polygon statistics and noted the mean pixel value and standard deviation within the polygon in each spectral band. To normalize the measurements from the bears across the flights/image sets, for each band in

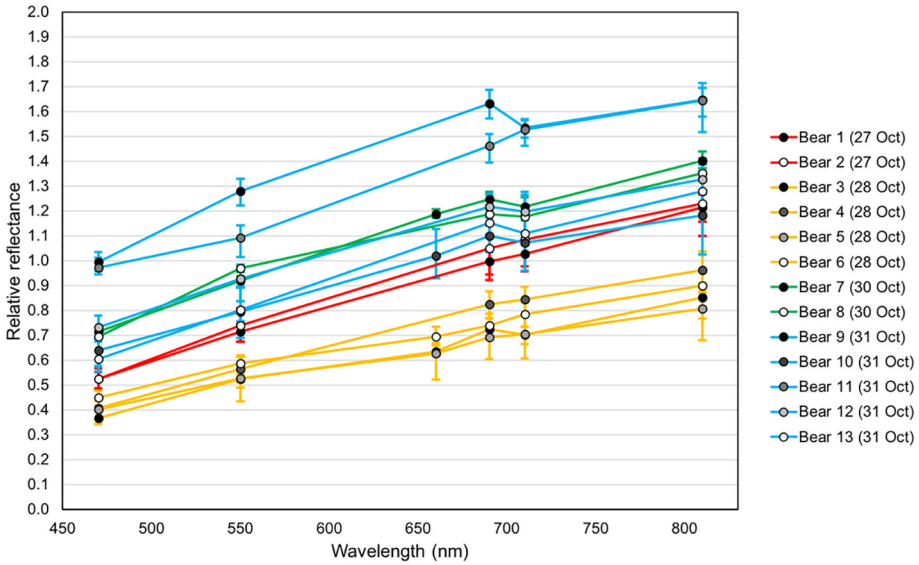

Fig. 1. Spectral reflectance curves (relative to the calibration tile) of adult polar bears imaged with a drone-borne multispectral camera in Churchill, MB, Canada, October 2014. Points represent the average reflectance of the bears across several measured images (calculated from the mean of each image); error bars represent the range of mean reflectance across the images. Large differences in measured reflectance among the bears likely resulted from variation in the camera's temperature; measurements from 28 October (orange curves) are likely closest to true absolute reflectance (see text). (For interpretation of the references to color in this figure legend, the reader is referred to the web version of this article.)

each image we divided the mean pixel value of the bear by the mean pixel value of the calibration tile imaged before the flight, so as to express the reflectance of the bear in relation to the tile.

Due to miscalibration of the camera's 660-nm (red) channel, which caused higher relative exposure in this band than the others, images from this channel were oversaturated and unusable for eight out of the 13 analyzed image sets. In addition, during preliminary analyses, we noted that the brightness of the bears sometimes exceeded that of the calibration tile, particularly in the longer-wavelength bands, which is anomalous since the tile is designed to reflect ~100% of incident radiation from ~400–1000 nm. Upon careful consideration of possible causes of these anomalies, we hypothesized that they likely resulted from having transported the drone-mounted camera inside the heated Tundra Buggy on 27, 30 and 31 October. Prior to each deployment, the temperature of the camera would have been much higher than the outdoor temperature and begun to cool upon being removed from the bus. Since the calibration tile was imaged very shortly (< 2 min) after the camera was taken outside, we believe the camera was likely still cooling down between the acquisition of the images of the tile and those of the bear several minutes later. This cooling may have increased the sensitivity of the image sensors, resulting in the images of the bear exceeding the brightness of the tile. This hypothesis is supported by the fact that the only image sets in which this anomaly did not occur were collected on the day that the drone and camera were transported in the bed of a pickup truck (28 October), where the camera would have remained at the cooler outdoor temperature. Thus, only measurements from the images captured on 28 October can likely be regarded as approximating the true reflectance of polar bears. Nevertheless, our results suggest the other images provide an accurate assessment of the relative brightness among bands.

To assess other landscape and background features for spectral resemblance to polar bears, we performed a supervised classification of each of the selected images of bears (totaling 76 images across 13 flights). For each image, we created two classes, “bear” and “background”. We traced the entire contour of the bear to serve as a training sample for the “bear” class, and used the entire rest of the image as a training sample for the “background” class. We then used the Maximum Likelihood algorithm (Richards, 2013) to classify every pixel in the image as either “bear” or “background” (according to the greatest likelihood of belonging to either of the normally-distributed class spectral signatures modelled from the training samples) with a probability threshold of 0.5001, meaning that only pixels calculated to have > 50% probability of belonging to either of the two classes were classified, while pixels that did not meet this threshold were left unclassified. This approach therefore revealed which background elements squarely overlapped with the spectral signature of the bear, as indicated by background pixels misclassified as “bear”; while also providing an assessment of the cohesiveness (i.e. the variation in the distribution) of the bear's spectral signature, as indicated by the proportion of pixels comprising the bear that were classified as “bear”. For the five image sets in which the 660-nm band was usable, we performed classifications both with and without the band to assess its impact on results.

As a broader supplemental analysis, we manually created a classification rule set for each image set (i.e. each flight) based on the measurements from the bear imaged during that flight. Among the previously selected images from which measurements were made, for each spectral band we used the image in which the bear's mean pixel value minus one standard deviation produced the lowest value to set the lower threshold for classifying pixels as “bear”; and used the image in which the bear's mean pixel value plus one standard deviation produced the highest value to set the upper threshold. We then used the IDL scripting application to batch-process all images containing the bear from each flight (totaling 786 images, ranging from 8 to 163 per flight) with the established rule set, generating classifications for each individual band as well as for all bands combined. For each classified image, we noted the total percentage of pixels classified as “bear” and documented background features that had been misclassified. The purpose of this analysis was to provide a general idea of which band(s) best distinguished bears from the background in the different landscapes in which they were imaged.

3. Results

The spectral reflectance curves of all imaged adult polar bears relative to the calibration tile are shown in Fig. 1. As a result of the temperature-related camera calibration issues described above, there was significant variation among the bears in their apparent overall brightness, although the shape of their reflectance curves was generally consistent. The distinctly high curves of two of the bears imaged on 31 October (Fig. 1, bears 9 and 11) likely resulted from variable sky conditions that day, with the calibration tile imaged under cloud cover and the bears subsequently imaged under clearer conditions several minutes later. The reflectance curves obtained for the bears imaged on 28 October, which are likely closest to the true reflectance of polar bears, showed an overall increase in reflectance with increasing wavelength, with average reflectance increasing from ~0.35–0.45 at 470 nm, to ~0.50–0.60 at 550 nm, ~0.60–0.70 at 660 nm, ~0.70–0.85 at 690 nm,

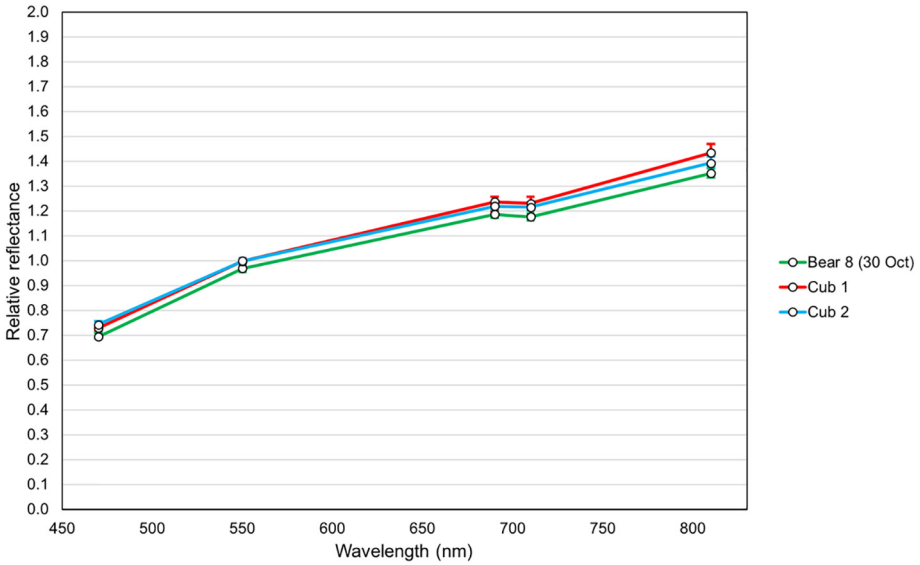

Fig. 2. Spectral reflectance curves (relative to the calibration tile) of an adult female polar bear with two cubs imaged with a drone-borne multispectral camera in Churchill, MB, Canada, 30 October 2014. Points represent the average reflectance of the bears across several measured images (calculated from the mean of each image); error bars represent the range of mean reflectance across the images.

marginally higher at 710 nm, and peaking at ~0.80–0.95 at 810 nm (Fig. 1). One noticeable characteristic was the presence of a small "bump" in reflectance at 690 nm followed by a slight drop at 710 nm for some of the bears but not the others (Fig. 1). No evident difference between the bears presenting this bump and those that did not could be visually discerned in the images. The reflectance curves of the cubs were similar to those of the adults, only marginally exceeding the brightness of the accompanying adult female in all bands (Fig. 2).

The results of the supervised classification analysis are summarized in Table 1. Given the varying altitude above ground from which images were captured, the number of pixels comprising the polar bear ranged from 28 to 9048 (median = 1080) of the ~1.3 million total pixels in each image. The proportion of bear pixels classified as "bear" with a probability threshold of 0.5001 was > 50% in all but two images (49.6% and 49.7%, respectively), with a maximum of 65.8%, and an average of 56.5% among all image sets (Table 1). Bear pixels misclassified as "background" only occurred in 14 out of 76 images and in negligible numbers, in all cases affecting < 1% of the pixels comprising the bear. All other bear pixels were labelled "unclassifiable". The proportion of background pixels misclassified as "bear" averaged < 0.01% in 10 out of 13 image sets, of which five image sets had < 0.001% misclassified pixels, and two image sets had no misclassified background pixels (Table 1). In only four out of 76 images did the proportion of background pixels misclassified as "bear" approach or exceed 0.1%, with 1225, 1847, 5992 and 8516 misclassified pixels, respectively. The latter two images were the lowest-altitude shots of Bear 2 (27 October), in which a significant amount of rocks and gravel in the surrounding landscape was misclassified as "bear" (Fig. 3). The next most prevalent misclassified background elements were small scatterings of vegetation embedded with snow, with the most severely affected image (1847 misclassified pixels) shown in Fig. 4. Notably, areas of pure snow did not appear to be affected by misclassification, as exemplified in Fig. 5. Including the red band (660 nm) in the analysis for the five image sets in which it was usable only yielded a marginal improvement in the proportion of bear pixels classified as "bear", with an average increase of 0.3–2.3 percentage points within each image set. Inclusion of the red band made no difference in the number of background pixels misclassified as "bear" in three image sets, while yielding an overall negligible decrease (−165 pixels across six images) and negligible increase (+41 pixels across six images) in misclassified pixels in the two other image sets, respectively.

Comparing the total proportion of each image classified as "bear" among the individual spectral bands across images captured in the different landscapes provides a general idea of which band(s) best distinguished the bears and which band(s) presented the most overlap between bears and background in each type of landscape (see Figs. A1–A4 in appendix). Overall, the results suggest that the bears were best distinguished from the background in the rock/gravel-dominated landscapes in the near-infrared band (810 nm), and relatively more poorly distinguished at shorter wavelengths (blue and green,

Table 1
Summary results of the supervised classification (Maximum Likelihood with probability threshold of 0.5001) of 1.3-megapixel aerial multispectral images (bands: 470 nm, 550 nm, 690 nm, 710 nm and 810 nm) of polar bears captured from a drone in Churchill, MB, Canada, October 2014, to assess the potential to differentiate bears from background.

Subject (date)	No. of images	No. of bear pixels/image	Average % of bear pixels classified as "bear" (range)	Average % of background pixels classified as "bear" (range)
Bear 1 (27 Oct)	6	198–284	52.4% (49.6–54.9%)	0.0004% (0.0000–0.0017%)
Bear 2 (27 Oct)	6	28–1499	54.1% (50.4–58.9%)	0.1856% (0.0000–0.6511%)
Bear 3 (28 Oct)	6	565–1576	53.3% (50.8–55.3%)	0.0058% (0.0011–0.0106%)
Bear 4 (28 Oct)	6	1759–8826	54.8% (51.6–57.5%)	0.0292% (0.0001–0.1424%)
Bear 5 (28 Oct)	6	189–1335	54.6% (52.4–57.3%)	0.0001% (0.0000–0.0006%)
Bear 6 (28 Oct)	6	1237–9048	55.2% (51.5–57.9%)	0.0000% (−)
Bear 7 (30 Oct)	6	660–1768	53.6% (52.0–55.2%)	0.0000% (−)
Bear 8 (30 Oct)	6	1369–1924	57.0% (55.9–57.9%)	0.0009% (0.0003–0.0016%)
Bear 9 (31 Oct)	6	430–1063	59.1% (49.7–63.9%)	0.0072% (0.0010–0.0114%)
Bear 10 (31 Oct)	6	738–1432	59.1% (51.7–65.8%)	0.0035% (0.0000–0.0155%)
Bear 11 (31 Oct)	6	392–1239	60.4% (55.7–64.3%)	0.0012% (0.0000–0.0053%)
Bear 12 (31 Oct)	4	254–2097	58.4% (52.9–62.2%)	0.0434% (0.0030–0.0935%)
Bear 13 (31 Oct)	6	731–2416	62.0% (60.9–64.4%)	0.0065% (0.0015–0.0212%)

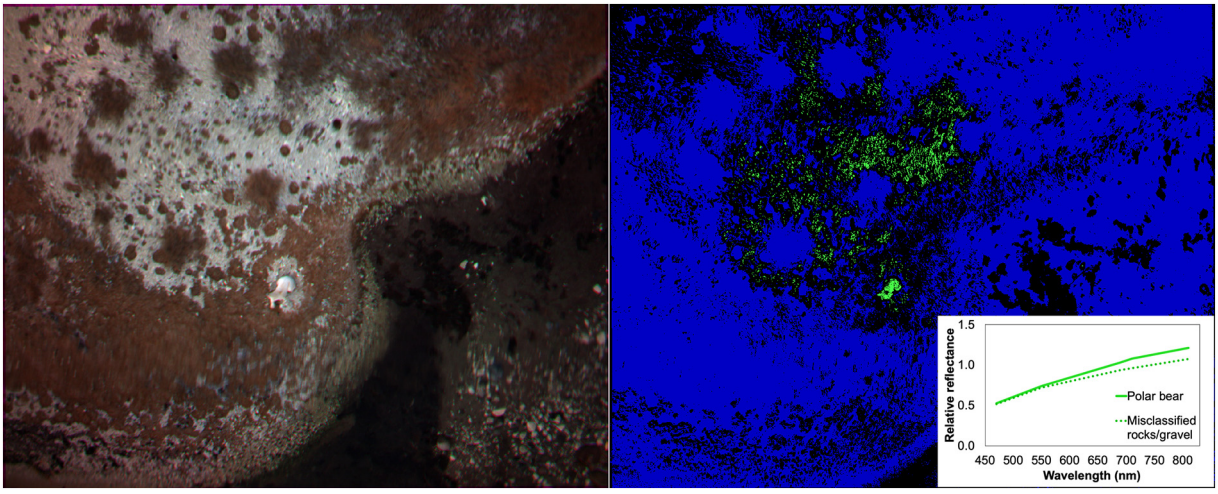

Fig. 3. Example of areas of rocks and gravel misclassified as "bear" by the Maximum Likelihood algorithm with a probability threshold of 0.5001 in a multispectral image (bands: 470 nm, 550 nm, 690 nm, 710 nm and 810 nm) of a polar bear captured from a drone in Churchill, MB, Canada, 27 October 2014. A simulated natural-color composite of the raw image is shown on the left and the classified image on the right, with pixels classified as "bear" in green, pixels classified as "background" in blue, and unclassifiable pixels in black. The plot compares the spectral reflectance curve of the bear to that of a manually sampled area of rocks and gravel of similar dimensions to the bear containing a high density of pixels misclassified as "bear". (For interpretation of the references to color in this figure legend, the reader is referred to the web version of this article.)

470–550 nm) (Fig. A1). In the vegetation-dominated landscapes, the blue and green bands were also relatively poor at distinguishing the bears, although in this case the red and red-edge bands (660–710 nm) tended to better distinguish the bears than the near-infrared band (Fig. A2). In contrast, the blue and green bands (and red when available) generally tended to best distinguish the bears in the snowy landscapes, with overall poorer differentiation at longer wavelengths, markedly at 710 nm and 810 nm (Fig. A3).

4. Discussion

We used a drone-borne multispectral camera to evaluate the potential to identify polar bears using remotely sensed multispectral imagery, such as could be obtained from satellites or high-altitude aerial photography. Despite some technical challenges with our equipment, we found that spectral reflectance patterns were generally similar to those previously reported by Leblanc et al. (2016), with bears reflecting light much more strongly in the red than the blue end of the spectrum. We further found that only a limited portion of the background in the natural landscapes in which we imaged the bears had similar reflectance patterns to bears.

Compared to the curves obtained by Grojean et al. (1980) and Leblanc et al. (2016) from polar bear pelts, the curves we obtained had a similar shape in the visible region (470–660 nm), with reflectance values in the properly calibrated imagery captured on 28 October overall slightly lower than those measured in the former study and slightly higher than those measured in the latter study. However, whereas the reflectance of the pelts in both previous studies began to rapidly plateau just beyond the visible red region, the curves we obtained did not show this plateauing, overall continuing to increase fairly steadily to a peak of ~0.80–0.95 in the 810-nm near-infrared band, compared to ~0.85 for the pelt measured by Grojean et al. (1980)

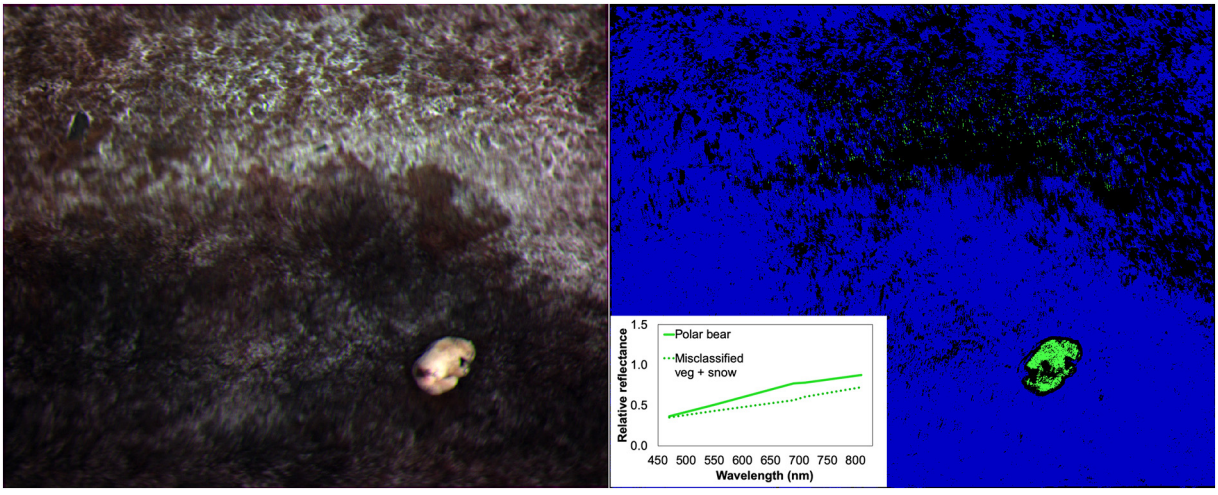

Fig. 4. Example of small scatterings of dead/senescing vegetation embedded with snow misclassified as "bear" by the Maximum Likelihood algorithm with a probability threshold of 0.5001 in a multispectral image (bands: 470 nm, 550 nm, 690 nm, 710 nm and 810 nm) of a polar bear captured from a drone in Churchill, MB, Canada, 28 October 2014. A simulated natural-color composite of the raw image is shown on the left and the classified image on the right, with pixels classified as "bear" in green, pixels classified as "background" in blue, and unclassifiable pixels in black. The plot compares the spectral reflectance curve of the bear to that of a manually sampled area of snow-embedded vegetation of similar dimensions to the bear containing a high density of pixels misclassified as "bear". (For interpretation of the references to color in this figure legend, the reader is referred to the web version of this article.)

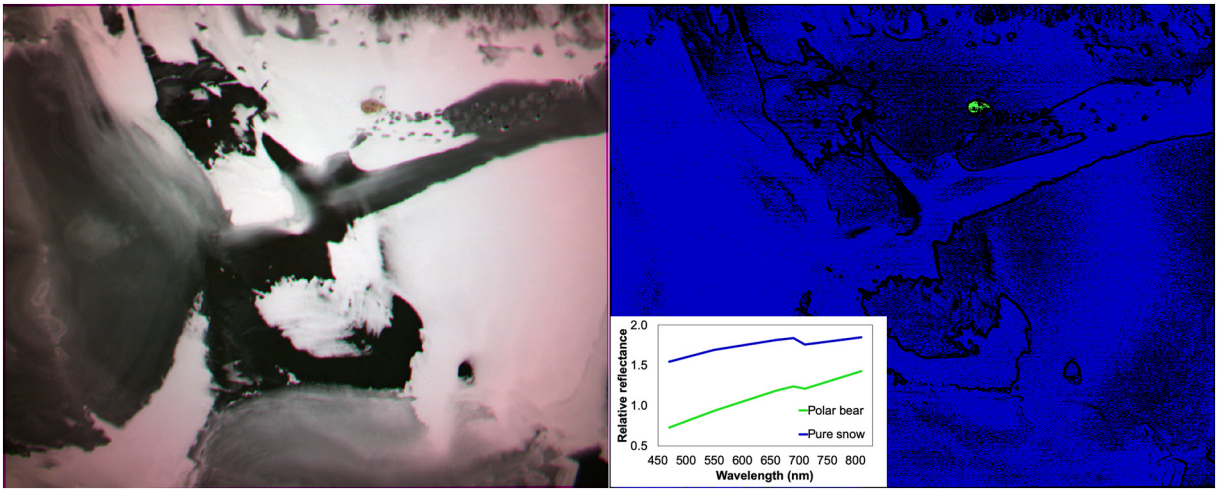

Fig. 5. Example of the clear spectral differentiation between a polar bear and pure snow by the Maximum Likelihood classification algorithm with a probability threshold of 0.5001 in a multispectral image (bands: 470 nm, 550 nm, 690 nm, 710 nm and 810 nm) captured from a drone in Churchill, MB, Canada, 30 October 2014. A simulated natural-color composite of the raw image is shown on the left and the classified image on the right, with pixels classified as "bear" in green, pixels classified as "background" in blue, and unclassifiable pixels in black. No background pixels were misclassified as "bear". The plot compares the spectral reflectance curve of the bear to that of a manually sampled area of pure snow next to and of similar dimensions to the bear. (For interpretation of the references to color in this figure legend, the reader is referred to the web version of this article.)

and ~0.55–0.65 for those measured by Leblanc et al. (2016). This discrepancy in the red-edge to near-infrared region may be due to effects of preparation or long-term storage of the pelts, or possibly due to the pelts having been collected at a different time of year (information on the timing of collection was not available for the pelts used in those studies). The among-bear variation in reflectance that we observed for the bears imaged on 28 October—from ~0.10–0.15 in each band—is also comparable to the variation among the pelts measured by Leblanc et al. (2016). The reflectance curves we measured from the bears imaged on 27, 30 and 31 October had similar shapes despite being overall brighter to varying degrees than the curves measured from the bears on 28 October. The curves measured from the two cubs had an identical shape to the accompanying adult female but were slightly brighter in all bands.

The Maximum Likelihood classification analysis provided an instructive appraisal of landscape background features that present a similar spectral signature to the polar bears, as well as of the degree to which the bears' spectral signature forms a tight profile, allowing for more precise and confident detection. Based on spectral reflectance alone, our results suggest that landscape features that most closely resemble bears in the visible to near-infrared region are bright rocks and gravel as well as snow-embedded vegetation. Regarding the latter, our supplemental analysis of the individual spectral bands suggests that polar bears are relatively more poorly distinguished from vegetation at shorter wavelengths (blue and green), while it is the reverse for pure snow. It is therefore unsurprising that a certain mixture of vegetation (tending to overlap with bears in the blue-green region) and snow (tending to overlap with bears toward the near-infrared region) can produce a similar spectral signature to polar bears. However, even in the image that was most severely affected by this type of misclassification (Fig. 4), the errors amounted to an extremely sparse scattering of pixels compared to the large and dense cluster of correctly classified pixels on the bear itself. It is doubtful that such small scatterings would register at all in coarser spatial-resolution satellite imagery, their signature diluted by other elements sharing the same pixel space. Similarly, only in the finest-scale images containing bright rocks and gravel were significant numbers of pixels representing these elements misclassified as "bear", suggesting that in the higher-altitude shots—and by extension in coarser satellite imagery—the confounding signature is diluted and lost. Nevertheless, the possibility of larger rocks or boulders being confounded with polar bears in wider-ranging imagery cannot be ruled out.

Our finding that a consistent proportion of ~50% or more of pixels comprising the bears were correctly classified by the Maximum Likelihood algorithm with a probably threshold of 0.5001 is also promising for detection of polar bears in coarser satellite imagery. In practical terms, these results mean that the bulk of the spectral signature produced by individual bears is narrow enough (in terms of distribution of values) that, on average, more than half of their overhead surface area can be matched to their core signature with a confidence level of > 50%. Combined with our finding that the remaining pixels comprising the bears were only misclassified as "background" in negligible numbers (with the overwhelming majority labelled "unclassifiable"), this suggests that the distinctive spectral signature of polar bears is less likely to become unrecognizably diluted in coarser imagery in the same way as the smaller-grain confounding background elements discussed above.

Overall, our results suggest that, provided a sufficient spatial resolution, use of multispectral remote sensing imagery to survey polar bears could eliminate many of the most frequent false positive errors reported in studies that used panchromatic imagery (Stapleton et al., 2014a; LaRue et al., 2015; LaRue and Stapleton, 2018), notably snow and ice. Currently, the best-suited earth observation satellite for potential multispectral detection of polar bears is DigitalGlobe's WorldView-3 (Toth and Józków, 2016), whose blue (450–510 nm), green (510–580 nm), red (630–690), red-edge (705–745 nm) and near-infrared 1 (770–895 nm) bands collectively encompass the wavelengths we analyzed in this study (WorldView-4, equipped with similar sensors, suffered an instrument failure in January 2019 that rendered the system inoperable). In addition, it has a "coastal" blue sensor (400–450 nm), a yellow sensor (585–625 nm) and a second near-infrared sensor (860–1040 nm) that could potentially further improve differentiation of polar bears from background features. We note, however, that although the 1.2-m spatial resolution of WorldView-3's multispectral sensors is finer than the 2.4-m WorldView-2 imagery deemed too coarse by LaRue et al. (2015), a polar bear would only be comprised of 3–4 pixels at most, which still may not be sufficient to reliably detect its distinctive spectral signature. Nevertheless, the spatial resolution of satellite imagery will likely continue to improve, making this application, as well as the detection of other wildlife species, increasingly practicable.

Ultimately, the ideal analytical approach to a "blind" survey of polar bears in large volumes of radiometrically calibrated multispectral

satellite imagery would be to identify features presenting the characteristic spectral curve of bears (Fig. 1)—with more emphasis on the reflectance ratios among the bands than on absolute reflectance values—in the framework of an object-based image analysis (OBIA) that would additionally filter out objects that do not match the size of polar bears. OBIA software has become increasingly accessible in recent years, now allowing fairly straightforward workflows for detecting wildlife in aerial imagery to be implemented by non-experts in remote sensing (Chabot et al., 2018). Complementary use of image differencing on multitemporal imagery could further reduce false positive errors (LaRue and Stapleton, 2018).

Drones provide a valuable means of collecting very close-range aerial imagery of otherwise difficult-to-approach wildlife, while causing minimal disturbance to animals if operated responsibly (Mulero-Pázmány et al., 2017). Aside from the first bear we surveyed that walked away from its resting spot in apparent reaction to the drone, all subsequent bears—initially approached at higher altitude than the first—did not superficially appear to be significantly disturbed, with reactions limited to shifting their posture and occasionally looking up at the drone. Similarly, a recent study by Barnas et al. (2018) found that vigilance behaviour displayed by polar bears that were approached by a drone did not significantly differ from their behaviour during typical tourist viewing activities in Churchill, Manitoba. Our field work took place at the tail end of a period during the initial proliferation of drones when options for employing multispectral cameras were very limited and poorly optimized for the application. The Mini-MCA6 we used was originally released in 2009 and was not well suited for the fast-motion and turbulent shooting conditions typical of drone-borne operation, resulting in frequent image blur. In recent years, multispectral cameras for use on drones have become more numerous in makes and models, more affordable, and significantly improved in terms of shutter and exposure performance, miniaturization, and ease of use (Manfreda et al., 2018). Furthermore, an increasing number of models are now equipped with an accessory incident light sensor that records ambient downwelling irradiance levels simultaneously with image capture for calibration of the imagery, as an alternative to relying on a calibration tile imaged before or after the flight. Given these favorable developments, drones could potentially be used to collect data on the spectral signatures of a variety of wildlife species that may be detectable in satellite imagery.

Declaration of Competing Interest

The authors declare no conflict of interest.

Acknowledgements

Funding for field work was provided by Environment and Climate Change Canada, as well as a subsidy from the Build in Canada Innovation Program to ING Robotic Aviation in support of several projects to evaluate the use of drones for environmental applications. The drone used in the study was operated by Edward McMann and Guy Gingras in accordance with a Special Flight Operations Certificate issued by Transport Canada. Polar Bears International provided logistical support in Churchill, MB, including accommodation, meals and an operator for the Tundra Buggy, which was loaned to the project by Frontiers North. We are particularly grateful to Geoff York and B.J. Kirschoffer for their assistance with field work and logistical support. We thank Todd Arnold (University of Minnesota) for his support of this work. Field research protocols were approved by the University of Minnesota's Institutional Animal Care and Use Committee (1207A17284). We finally thank John Edling of Tetracam Inc. for technical support and insight during image processing and analysis.

Appendix A. Supplementary data

Supplementary data to this article can be found online at https://doi.org/10.1016/j.biocon.2019.06.022.

References

Barber-Meyer, S.M., Kooyman, G.L., Ponganis, P.J., 2007. Estimating the relative abundance of emperor penguins at inaccessible colonies using satellite imagery. Polar Biol. 30 (12), 1565–1570.
Barnas, A.F., Felege, C.J., Rockwell, R.F., Ellis-Felege, S.N., 2018. A pilot(less) study on the use of an unmanned aircraft system for studying polar bears (*Ursus maritimus*). Polar Biol. 41 (5), 1055–1062.
Chabot, D., Bird, D.M., 2015. Wildlife research and management methods in the 21st century: where do unmanned aircraft fit in? J. Unman. Veh. Syst. 3 (4), 137–155.
Chabot, D., Dillon, D., Francis, C.M., 2018. An approach for using off-the-shelf object-based image analysis software to detect and counts birds in large volumes of aerial imagery. Avian Conserv. Ecol. 13 (1), 15.
Fretwell, P.T., Staniland, I.J., Forcada, J., 2014. Whales from space: counting southern right whales by satellite. PLoS One 9 (2), e88655.
Fretwell, P.T., Scofield, P., Phillips, R.A., 2017. Using super-high resolution satellite imagery to census threatened albatrosses. Ibis 159 (3), 481–490.
Grojean, R.E., Sousa, J.A., Henry, M.C., 1980. Utilization of solar radiation by polar animals: an optical model for pelts. Appl. Opt. 19 (3), 339–346.
He, K.S., Bradley, B.A., Cord, A.F., Rocchini, D., Tuanmu, M.-N., Schmidtlein, S., Turner, W., Wegmann, M., Pettorelli, N., 2015. Will remote sensing shape the next generation of species distribution models? Remote Sens. Ecol. Conserv. 1 (1), 4–18.
Hughes, B.J., Martin, G.R., Reynolds, S.J., 2011. The use of Google Earth satellite imagery to detect the nests of masked boobies *Sula dactylatra*. Wildl. Biol. 17 (2), 210–216.
Kerr, J.T., Ostrovsky, M., 2003. From space to species: ecological applications for remote sensing. Trends Ecol. Evol. 18 (6), 299–305.
Laidre, K.L., Stern, H., Born, E.W., Heagerty, P., Atkinson, S., Wiig, Ø., Lunn, N.J., Regehr, E.V., McGovern, R., Dyck, M., 2018. Changes in winter and spring resource selection by polar bears *Ursus maritimus* in Baffin Bay over two decades of sea-ice loss. Endanger. Species Res. 36, 1–14.
LaRue, M.A., Stapleton, S., 2018. Estimating the abundance of polar bears on Wrangel Island during late summer using high-resolution satellite imagery: a pilot study. Polar Biol. 41 (12), 2621–2626.
LaRue, M.A., Rotella, J.J., Garrott, R.A., Siniff, D.B., Ainley, D.G., Stauffer, G.E., Porter, C.C., Morin, P.J., 2011. Satellite imagery can be used to detect variation in abundance of Weddell seals (*Leptonychotes weddellii*) in Erebus Bay, Antarctica. Polar Biol. 34 (11), 1727–1737.
LaRue, M.A., Stapleton, S., Porter, C., Atkinson, S., Atwood, T., Dyck, Lecomte, N., 2015. Testing methods for using high-resolution satellite imagery to monitor polar bear abundance and distribution. Wildl. Soc. Bull. 39 (4), 772–779.
LaRue, M.A., Stapleton, S., Anderson, M., 2017. Feasibility of using high-resolution satellite imagery to assess vertebrate wildlife populations. Conserv. Biol. 31 (1), 213–220.
Leblanc, G., Francis, C.M., Soffer, R., Kalacska, M., de Gea, J., 2016. Spectral reflectance of polar bear and other large arctic mammal pelts; potential applications to remote sensing surveys. Remote Sens. 8 (4), 273.
Lunn, N.J., Servanty, S., Regehr, E.V., Converse, S.J., Richardson, E., Stirling, I., 2016. Demography of an apex predator at the edge of its range: impacts of changing sea ice on polar bears in Hudson Bay. Ecol. Appl. 26 (5), 1302–1320.
Lynch, H.J., White, R., Black, A.D., Naveen, R., 2012. Detection, differentiation, and abundance estimation of penguin species by high-resolution satellite imagery. Polar Biol. 35 (6), 963–968.
Manfreda, S., McCabe, M.F., Miller, P.E., Lucas, R., Madrigal, V.P., Mallinis, G., Dor, E.B., Helman, D., Estes, L., Ciraolo, G., Müllerovà, J., Tauro, F., De Lima, M.I., De Lima, J.L.M.P., Maltese, A., Frances, F., Caylor, K., Kohv, M., Perks, M., Ruiz-Pérez, G., Su, Z., Vico, G., Toth, B., 2018. On the use of unmanned aerial systems for environmental monitoring. Remote Sens. 10 (4), 641.
McMahon, C.R., Howe, H., van den Hoff, J., Alderman, R., Brolsma, H., Hindell, M.A., 2014. Satellites, the all-seeing eyes in the sky: counting elephant seals from space. PLoS One 9 (3), e92613.
Mulero-Pázmány, M., Jenni-Eiermann, S., Strebel, N., Sattler, T., Negro, J.J., Tablado, Z., 2017. Unmanned aircraft systems as a new source of disturbance for wildlife: a systematic review. PLoS One 12 (6), e0178448.
Regehr, E.V., Lunn, N.J., Amstrup, S.C., Stirling, I., 2007. Effects of earlier sea ice breakup on survival and population size of polar bears in Western Hudson Bay. J. Wildl. Manag. 71 (8), 2673–2683.
Regehr, E.V., Hostetter, N.J., Wilson, R.R., Rode, K.D., St. Martin, M., Converse, S.J., 2018. Integrated population modeling provides the first empirical estimates of vital rates and abundance for polar bears in the Chukchi Sea. Sci. Rep. 8, 16780.
Richards, J.A., 2013. Supervised classification techniques. In: Richards, J.A. (Ed.), Remote Sensing Digital Image Analysis: An Introduction, Fifth edition. Springer-Verlag, Heidelberg, Germany, pp. 247–318.
Sasamal, S.K., Chaudhury, S.B., Samal, R.N., Pattanaik, A.K., 2008. QuickBird spots flamingos off Nalabana Island, Chilika Lake, India. Int. J. Remote Sens. 29 (16), 4865–4870.
Schmidt, A.L., Clark, D.A., 2018. “It's just a matter of time:” lessons from agency and community responses to polar bear-inflicted human injury. Conserv. Soc. 16 (1), 64–75.
Stapleton, S., LaRue, M., Lecomte, N., Atkinson, S., Garshelis, D., Porter, C., Atwood, T.,

2014a. Polar bears from space: assessing satellite imagery as a tool to track Arctic wildlife. PLoS One 9 (7), e101513.
Stapleton, S., Atkinson, S., Hedman, D., Garshelis, D., 2014b. Revisiting Western Hudson Bay: using aerial surveys to update polar bear abundance in a sentinel population. Biol. Conserv. 170, 38–47.
Stirling, I., 2011. Polar Bears: The Natural History of a Threatened Species. Fitzhenry & Whiteside, Markham, Ontario, Canada.
Toth, C., Józków, G., 2016. Remote sensing platforms and sensors: a survey. ISPRS J. Photogramm. Remote Sens. 115, 22–36.
Xue, Y., Wang, T., Skidmore, A.K., 2017. Automatic counting of large mammals from very high resolution panchromatic satellite imagery. Remote Sens. 9 (9), 878.
Yang, Z., Wang, T., Skidmore, A.K., de Leeuw, J., Said, M.Y., Freer, J., 2014. Spotting east African mammals in open savannah from space. PLoS One 9 (12), e115989.